THE JOURNAL OF PHYSICAL CHEMISTRY A

ARTICLE

pubs.acs.org/JPCA

Electron Correlation Effects on the Femtosecond Dephasing Dynamics of E_{22} Excitons in (6,5) Carbon Nanotubes

J. R. Schneck,[†,§] A. G. Walsh,[‡,§] A. A. Green,[⊥] M. C. Hersam,[⊥,#] L. D. Ziegler,[*,†,§] and A. K. Swan[*,‡,§,∥]

[†]Department of Chemistry and [‡]Department of Physics, 590 Commonwealth Avenue, Boston University, Boston, Massachusetts 02215, United States

[§]The Photonics Center and [∥]Department of Electrical and Computer Engineering, 8 Saint Mary's Street, Boston University, Boston, Massachusetts 02215, United States

[⊥]Department of Material Science and Engineering and [#]Department of Chemistry, 2220 Campus Drive, Northwestern University, Evanston, Illinois 60208, United States

ABSTRACT: Highly nonlinear pump fluence dependence was observed in the ultrafast one-color pump−probe responses excited by 38 fs pulses resonant with the E_{22} transition in a room-temperature solution of (6,5) carbon nanotubes. The differential probe transmission ($\Delta T/T$) at the peak of the pump−probe response (τ = 20 fs) was measured for pump fluences from $\sim 10^{13}$ to 10^{17} photons/pulse cm^2. The onset of saturation is observed at $\sim 2 \times 10^{15}$ photons/pulse cm^2 ($\sim 8 \times 10^5$ excitons/cm). At pump fluences >4×10^{16} photons/pulse cm^2 ($\sim 1.6 \times 10^6$ excitons/cm), $\Delta T/T$ decreases as the pump fluence increases. Analogous signal saturation behavior was observed for all measured probe delays. Despite the high exciton density at saturation, no change in the E_{22} population decay rate was observed at short times (<300 fs). The pump probe signal was modeled by a third-order perturbation theory treatment that includes the effects of inhomogeneous broadening. The observed $\Delta T/T$ signal is well-fit by a pump-fluence-dependent dephasing rate linearly dependent on the number of excitons created by the pump pulse. Therefore, the observed nonlinear pump intensity dependence is attributed to the effects of quasi-elastic exciton−exciton interactions on the dephasing rates of single carbon nanotubes. The low fluence total dephasing time is 36 fs, corresponding to a homogeneous width of 36 meV (290 cm^{-1}), and the derived E_{22} inhomogeneous width is 68 meV (545 cm^{-1}). These results are contrasted with photon-echo-derived parameters for the E_{11} transition.

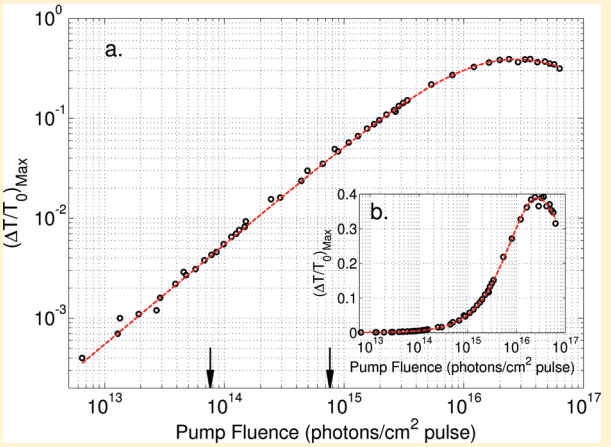

INTRODUCTION

Optical excitation of electron−hole pairs in semiconducting systems in the high fluence limit reveals information on carrier−carrier interactions such as dielectric screening, exciton binding energy and size, and lifetime and dephasing effects. For example, at high exciton densities, a Mott transition is expected, with bound excitons changing to an e-hole plasma.[1,2] In carbon nanotubes, the exciton binding energy is unusually large and, even in a screened environment such as a solution, the exciton binding energy is still on the order of ~0.5 eV.[3,4] Hence, one could expect that a larger number of excitons could be stable on a nanotube, as compared with nanowires that have lower binding energies and concomitant larger exciton sizes. Pump−probe studies at high fluence have reported excitation up to hundreds of excitons/tube showing fluence dependent population decay dynamics with increasing pump power.[5,6] Therefore, exciton interactions, either via scattering or Auger decay, are bound to be manifested in signal saturation,[5,6] relaxation dynamics,[5,7] and dephasing rates.[8−10] The fluence-dependent dephasing rate ($1/T_2$) can have contributions from both exciton quasi-elastic scattering (T_2^*) and population decay (T_1).

In this study, we report on single-color E_{22} resonant pump−probe measurements of a near pure solution of (6,5) carbon nanotubes.[11] The differential transmission signal, $\Delta T/T$, as a function of pump fluence shows not only saturation but also a decrease in the signal at the highest pump fluences used here. This saturation effect limits the exciton density to $\sim 1.6 \times 10^6$ excitons/cm. The sub-300 fs E_{22} pump−probe decay is found to be unaffected by the pump fluence, ruling out exciton population decay signal intensity limiting factor invoked in other studies.[12,13]

Special Issue: Graham R. Fleming Festschrift

Received: September 1, 2010
Revised: December 5, 2010
Published: January 11, 2011

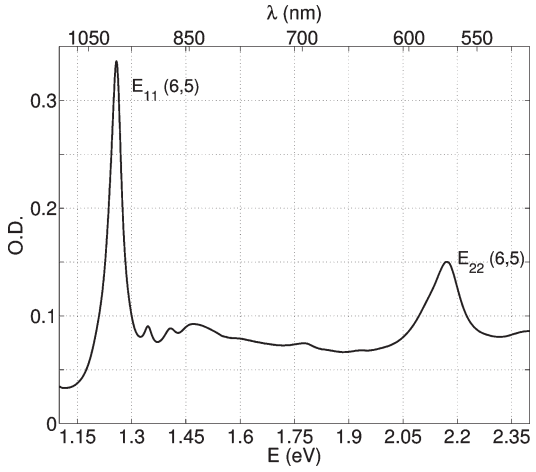

Figure 1. Extinction (absorption) spectrum of (6,5) nanotube solution in 1 mm path length cell. E_{11} and E_{22} electronic transition regions are indicated.

Third-order perturbation theory demonstrates that the magnitude of the $\Delta T/T$ signal is a function of the T_2 dephasing time scale when the incident pulse durations are longer than the electronic coherence loss time scale.[12,13] Therefore, careful measurement of differential probe transmission signals may be used, albeit indirectly, to obtain dephasing rate measurements when the overall resonant E_{22} absorption line width (including inhomogeneous broadening) is broader than the pulse width of the optically resonant radiation. Here, as described in greater detail below, the observed saturation behavior of the pump-dependent probe transmission at a fixed pump−probe interpulse time delay is attributed to an increase in the quasi-elastic dephasing rate $1/T_2^*$ with increasing fluence because T_1 effects can be ruled out by the kinetics measurements. This finding is supported by other studies that report fluence-independent E_{22} population dynamics at early times (less than hundreds of femtoseconds).[6,14]

The saturation and decrease in the fluence dependent $\Delta T/T$ signal reported here cannot be compared to high fluence photoluminescence (PL) saturation measurements that show similar trends, albeit at lower saturation fluences.[15] PL saturation probes the dynamics in the full E_{11} exciton dispersion band, whereas one-color pump−probe saturation studies of carbon nanotubes probe only the E_{ii} zero momentum state. For these reasons, we will not make direct comparisons between pump−probe and PL measurements.

EXPERIMENTAL PROCEDURES

Nanotube Sample. The experimental sample was a solution enriched in (6,5) single-walled carbon nanotube (SWNT) species produced by density gradient ultracentrifugation.[11,16] The final (6,5) enriched material was dialyzed into 1% w/v sodium cholate aqueous solution to remove the density gradient medium (iodixanol). Figure 1 shows the absorption spectrum (referenced to a sodium cholate solution), formally an extinction spectrum, with the E_{11} and E_{22} absorption energies for the (6,5) enriched nanotube sample evident at 1.26 (984 nm) and 2.17 eV (571 nm), respectively. This spectrum was obtained in a 1 mm path length cell. The observed corresponding fwhm values of these transitions are 35 meV/280 cm^{-1} (E_{11}) and 94 meV/750 cm^{-1} (E_{22}). The peak extinction coefficient of the E_{11} transition is ~3.5 times greater than that of the E_{22} band, although the integrated oscillator strength of the lower lying transition is approximately only 25% larger than the E_{22} transition, assuming that the extinction is dominated by absorption rather than scattering. (See below.) We attribute the weak broad baseline contributing to the spectrum (OD ≈ 0.05) to scattering and trace absorption. The nanotubes' length distribution was measured by multiple AFM images and can be approximated by a log-normal distribution with a median length of 600 nm, and the carbon nanotube density was $\rho \approx 1.6 \times 10^{14}$ cm^{-3}.[16]

Transition Moment Determination. For use of the pump−probe signal at a fixed interpulse delay as a measure of the resonance coherent relaxation dynamics (eqs 2 and 3), an accurate value of the resonant transition moment is required. For these ~600 nm SWNTs, the relative contribution of Mie scattering loss potentially complicates the simple interpretation of the extinction spectrum (Figure 1) in terms of the electronic absorption strength. The scattering contribution to the extinction coefficient at 571 nm was measured by referencing the observed scattering intensity of the 600 nm nanotube solution to two solutions: (1) the scattering of 600 nm polystyrene nanobeads as a standard for 100% scattering and (2) the scattering of water for ~0% background level of scattering at this wavelength. The concentration of 600 nm nanobeads was adjusted to match the optical density (OD) of the SWNT solution. The excitation source for these scattering measurements was the low-power 571 nm laser pulses used for the pump−probe measurements. Relative scattering measurements were made for these three samples, water, 0.15 OD nanobeads, and 0.15 OD SWNTs, as a function of viewing angle. After angle averaging, the extinction loss due to Mie light scattering accounts for only ~5% of the total observed for the E_{22} transition of this solution. This low percentage of light scattering compared with absorption has also been confirmed by recent scattering measurements.[17]

Therefore, the average E_{22} transition moment (per nanotube) is determined in the usual fashion by integrating the absorption spectrum (in SI units of inverse length)

$$|\mu|^2 = \frac{6\hbar c^2 \varepsilon_0 n}{\omega \rho} \int \alpha_{abs}(\tilde{\nu})\, d\tilde{\nu} \qquad (1)$$

where $\hbar$, ε_0, and c have their standard meanings, ρ is the density of nanotubes, ω is the E_{22} transition frequency, n is the solution index of refraction (taken as that of water at λ = 570 nm, n = 1.33), and the observed attenuation is reduced by 5% to take the scattering loss into account. The resulting E_{22} transition length, μ/e, is ~0.95 nm for this ensemble distribution. From the known nanotube number density of 1.6×10^{14} cm^{-3} and a (baseline-corrected) peak extinction of ~0.09 OD (1 mm path length) for our experimental sample, an peak absorption cross-section of $\sigma_{22} = 1.3 \times 10^{-14}$ cm^2/nanotube is determined after correcting for the ~5% scattering loss and is in agreement with previously reported σ_{22} values.[18] This ensemble result reflects the average over the tube length distribution.

Differential Pump−Probe Transmission Measurements. E_{22} resonant ultrafast pulses were produced by an optical parametric amplifier pumped by a 100 kHz Ti/sapphire regenerative amplifier system. One-color pump−probe measurements were performed with near-transform-limited Gaussian pulses of 38 fs pulse width, 52 meV (420 cm^{-1}), tuned to the E_{22} resonance at 571 nm. (See Figure 1.) The pump and probe pulse beams were

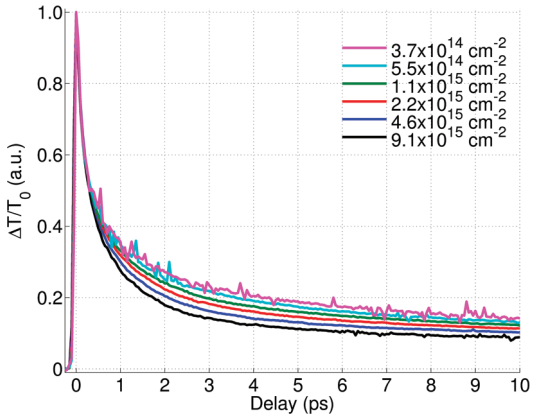

Figure 2. Observed E_{22} resonant pump−probe responses of (6,5) SWNTs excited by 38 fs pulses for the indicated range of pump pulse fluences. These responses have been normalized to the peak of the signal bleach for the range of pump fluences shown here. Note that the normalized responses are identical until delays of ∼300 fs.

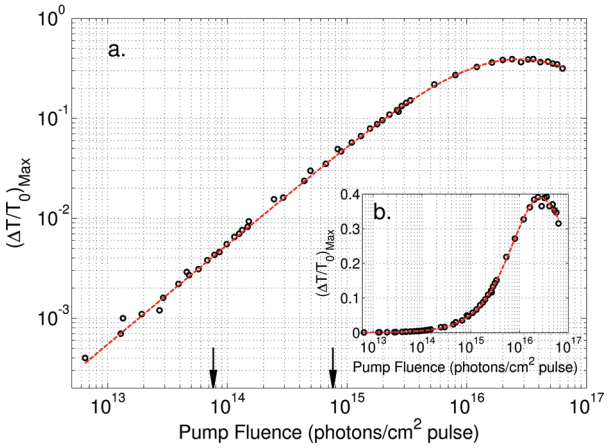

Figure 3. $(\Delta T/T_o)_{max}$ (τ = 20 fs delay) as a function of pump fluence. (a) Log−log plot of $(\Delta T/T_o)_{max}$ with fit from eq 2. The arrows indicate 1 and 10 exciton/nanotube, respectively. (b) Log−lin plot of $(\Delta T/T)_{max}$ with fit from eq 2 to emphasize the decrease in signal after saturation.

orthogonally polarized to minimize pump scatter contamination along the probe direction. A polarizer and half-wave plate combination controlled the large dynamic range of incident pump pulse intensities. The incident intensity beam waists (1/e) at the sample focus were determined by "knife edge" scans to be 18 μm with a confocal length of 900 μm. The crossing angle between pump and probe beams in the near-collinear experimental configuration was ∼5° in the sample (6.8° in air). Experiments were carried out in a 1 mm path-length room-temperature sample. The pump−probe signal was detected using a silicon photodiode and a lock-in amplifier. Care was taken to avoid apertures along the probe beam path before the detector to avoid any thermal lensing effects. The chopped probe beam transmission was independently calibrated to the locking signal to provide the required differential transmission $(\Delta T/T)$ ratio. For all measurements reported here the probe intensity was at least 20 times weaker than that of the pump, and the observed pump−probe signal was linear with respect to the probe pulse energy. Throughout the course of these studies, the OD of our nanotube solution remained constant, indicating the robustness of this sample to any significant optical or thermal degradation.

RESULTS AND DISCUSSION

Observed Pump−Probe Responses and Pump Pulse Fluence Dependence. The normalized E_{22} resonant pump probe responses of the (6,5) SWNT solution sample (Figure 1) excited by 38 fs pulses are shown in Figure 2 for a range of pump pulse fluences that span four orders of magnitude. For this one-color (571 nm) experiment, the pump−probe signal is a transient bleach response at all interpulse time delays (τ) and exhibits multiple decay components. A more detailed analysis of the population dynamics and the observed fluence dependence evident in these time-resolved responses will be given elsewhere. The peak of the bleach response appears for a time delay of ∼20 fs at all pump fluences. Although the observed E_{22} population relaxation dynamics are fluence-dependent, the pump−probe decay over the first ∼300 fs is fluence-independent, as seen in Figure 2. Hence, the E_{22} exciton lifetime T_1 is not affected by the pump fluence in the short time regime (<∼300 fs). A similar E_{22} decay time was reported in a recent study of near-single chirality samples.[19] In a previous study, significantly faster E_{22} population decay rates were reported.[20] However, we attribute this difference to the highly inhomogeneous and mixed chiral character of the sample used in that previous study, as evidenced by the nearly continuous absorption spectrum in the 1 to >3 eV range for that sample.[20]

The observed change in probe beam transmission $(\Delta T/T_o)_{max}$, defined as the power of the probe beam with the pump on (I_{on}) minus the probe beam power with the pump off (I_{off}) normalized by the probe power, $(I_{on} - I_{off})/I_{off}$, is plotted in Figure 3 as a function of incident pump pulse fluence for the fixed interpulse delay (τ) of 20 fs, which is the maximum of the observed transient response (Figure 2). The finite material response time of the SWNT system accounts for this short temporal offset from the pulse autocorrelation peak (τ = 0). Both log−log (Figure 3a) and semilog plots (Figure 3b) of this fluence dependence are displayed in this figure. The arrows indicate fluences where 1 and 10 excitons/nanotube are excited, respectively. The incident pump pulse fluence, reported as the number of pump pulse photons per beam 1/e area averaged over the sample length, was varied from ∼6×10^{12} to ∼6×10^{16} photons/cm^2 per pulse.

As seen in Figure 3a, $(\Delta T/T_o)_{max}$ increases linearly with pump power until ∼2×10^{15} photons/cm^2 pulse, where a saturation effect becomes evident in these log−log plots. Given the measured average E_{22} cross-section $\sigma_{22} = 1.3 \times 10^{-14}$ cm^2/nanotube, this incident intensity corresponds to the excitation of ∼25 excitons per nanotube. The nonlinear pump dependence results in the magnitude of $\Delta T/T_o$ reaching an absolute maximum (saturation) for a pump fluence of ∼4×10^{16} photons/cm^2, as seen in this Figure (∼100 excitons per nanotube or ∼1.6×10^6 excitons/cm). At fluences >4×10^{16} photons/cm^2, the measured response not only shows saturation but also decreases by almost 25% of the maximum $\Delta T/T_o$ value as the pump fluence is increased further to the largest values used in this study (6×10^{16} photons/cm^2 pulse).

This saturation and decrease in the $\Delta T/T_o$ signal was also found for delay times significantly far from the pump−probe pulse overlap region, as shown in Figure 4, where the $\Delta T/T_o$ signal for five interpulse delays (τ) in the range from 100 fs to 10

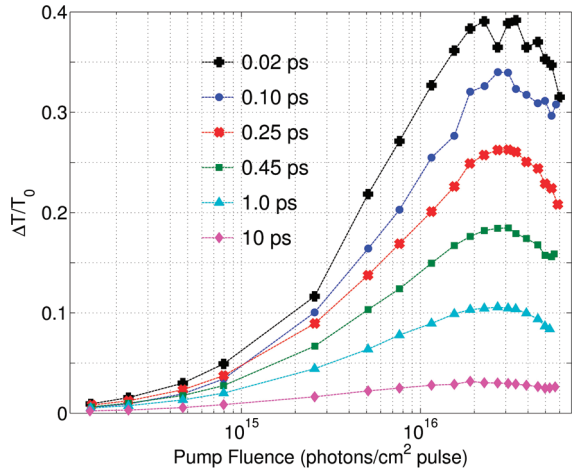

Figure 4. $\Delta T/T_o$ as a function of pump fluence for different delay times of the probe pulse, as indicated. The saturation and decrease remain well outside pump probe signal overlap.

ps are given. For comparison, the τ = 20 fs data (Figure 3b) are included here as well. The shape of this saturation-like behavior is qualitatively similar for all pump−probe interpulse delay times. Both the saturation and decrease in pump−probe signal are evident at these delay times well beyond the pulse duration, and thus the mechanism resulting in nonlinear pump fluence dependence for these pump−probe responses affects the signal amplitude for times well past the pump−probe temporal overlap region. As discussed below, this observation is important for establishing the nature of this pump fluence dependent effect.

Saturation effects in SWNT E_{22} pump−probe measurements have been attributed to exciton size effects, which limit the effective exciton population density due to Auger-type relaxation.[6] Auger-type relaxation accounting for $\tau \approx 0$ saturation can be ruled out because no change in E_{22} population decay rates is observed at early times (<300 fs) as a function of pump fluence. (See Figure 2.)

Ground-state depletion could also give rise to saturation effects at half filling according to the Einstein rate model.[21] The total number of available excitons in the E_{22} sub-band is given by the tube chirality and tube length, $2K_{CM}/\Delta K_{CM} = 2L/T \approx 300$ for average tube length L = 600 nm and translation vector T = 4 nm for a (6,5) nanotube.[22] (The factor of 2 comes from electronic degeneracy.) We note that saturation takes place below this number of excitons (300/2 excitons). Furthermore, such a mechanism cannot explain the observed decrease in $\Delta T/T$ for fluences >4 × 10^{16} photons/cm^2.

As describe below, we propose that a fluence-dependent quasi-elastic dephasing (T_2*) process be considered as the mechanism responsible for this pump−probe saturation behavior. As noted above, such T_2* fluence dependence is evident for the E_{11} transition of (6,5) nanotubes,[8,9] although such an effect on pump−probe intensities has not previously been considered. The quantitative dependence of the pump−probe signal on the rate of quasi-elastic dephasing in an inhomogeneously broadened two-level system is given below.

Pump−Probe Description. The change in the integrated intensity of a weak probe pulse due to a spatially overlapped pump pulse can be cast in terms of the unitless quantity, $\Delta T/T_o$, where ΔT is the difference in the transmission of the probe power at a detector after the sample, in the absence and presence of the pump ($\Delta T = T_{probe}^{pump\ on} - T_{probe}^{pump\ off}$) and T_o is just $T_{probe}^{pump\ off}$. In terms of the usual third-order polarization amplitude describing a pump probe response and the other relevant experimentally derived parameters for this system (in SI units), the differential transmission is given by (see the Appendix)

$$\frac{\Delta T(\tau)}{T_o} = \frac{4\omega/n^2 C_\theta \mathrm{Im}\int_{-\infty}^{\infty} dt\, E_{pr}^*(t) P^{(3)}(t,\tau)}{I_{probe}^o(10^{-OD})} \qquad (2)$$

where I_{probe}^o is the incident probe beam energy before the sample centered at ω. OD, ℓ, and n are the optical density, path length, and index of refraction of the nanotube solution respectively. C_θ is a geometrical factor accounting for the finite small angle between the near collinear pump and probe beams that reduces the number of nanotubes contributing to the $P^{(3)}$ signal (numerator) relative to the linear signal (denominator).

The familiar third-order pump−probe polarization response for the $E_{pu} - E_{pu} - E_{pr}$ time history is given by[13]

$$P^{(3)}(t,\tau) = \left(\frac{i}{\hbar}\right)^3 |\mu_{22}|^4 f_{1122}\rho^{(0)} \int_0^\infty\int_0^\infty\int_0^\infty dt_3\, dt_2\, dt_1\, E_{pu}(t-t_3-t_2-t_1) \times E_{pu}^*(t-t_3-t_2) \times E_{pr}(t-t_3-\tau) \times \exp\left(-\left(\gamma_2 t_1 + \frac{1}{2}\Delta_{in}^2 t_1^2\right)\right) e^{-t_2/T_1} \times \exp\left(-\left(\gamma_2 t_3 + \frac{1}{2}\Delta_{in}^2 t_3^2\right)\right) \qquad (3)$$

where μ_{22}, $\rho^{(0)}$, and f_{1122} are the E_{22} transition moment, nanotube density, and orientational averaging factor for perpendicularly polarized pump−probe beams in an otherwise isotropic sample.[23] Corresponding to this one-color experiment, the pump and probe fields have the same Gaussian time envelope but are temporally displaced and have different amplitude. T_1 represents the E_{22} excited state lifetime. The free induction decay (FID) of the resonant E_{22} electronic coherence is described here as resulting from both a homogeneous dephasing ($\gamma_2 = 1/T_2 = 1/T_2^* + 1/2T_1$) and an inhomogeneous broadening (Δ_{in}) contribution. For convenience, the inhomogeneous contribution is modeled as a static Gaussian distribution of transition frequencies, and the slight asymmetry in the absorption band shape is ignored. The effects of spectral diffusion are taken to be much slower than the time scale of the dephasing dynamics for this electronically coupled degree of freedom. Coherence relaxation dynamics during the pump and probe steps are distinguished by the t_1-and t_3-dependent exponentials in the $P^{(3)}$ expression (eq 3). For the finite pulse width analysis carried out here, the contributions of the other third-order density matrix pathways due to the nonsequential field histories ($E_{pu} - E_{pr} - E_{pu}$ and $E_{pr} - E_{pu} - E_{pu}$) are also analogously explicitly included in our modeling of the observed differential probe transmission due to overlapping pump and probe pulse histories (subpulse width delay τ).

Perhaps of greatest relevance to the data presented, in the rapid dephasing limit, where the width of the resonant absorption band is broader than the spectral breadth of the pump/probe pulses, the pump−probe signal appearing in the numerator of eq 2, neglecting the effects of inhomogeneous broadening, is proportional to[12]

$$\Delta T(\tau) \propto I_{pu} I_{pr} |\mu_{22}|^4 \frac{e^{-\tau/T_1}}{(1/T_2)^2} \qquad (4)$$

Therefore, for a fixed interpulse delay (τ) and well-characterized transition moment, the change in the transmitted probe pulse power is a sensitive function of the total dephasing dynamics of the resonant electronic coherence when these FID time scales are shorter than the pulse durations. As shown further below, the inclusion of a t^2-dependent contribution to the FID, that is, a static inhomogeneous contribution, does not affect this conclusion. The pump fluence dependence on the pump−probe signals thus may serve to characterize the dephasing dynamics of the resonant electronic transition when the material coherence loss time scale is shorter than the resonant pulse duration.

Modeling the Observed Pump Fluence Dependence (τ = 20 fs). From the qualitative relationship summarized by eq 4, pump−probe signals may provide a measure of subpulse width electronic dephasing time scales in the rapid dephasing limit. The observed 94 meV (750 cm^{-1}) E_{22} absorption width, relative to the 52 meV (420 cm^{-1}) pulsewidth, qualifies this experimental system for this rapid dephasing limit. This expression (eq 4) also reveals a possible explanation for the observed saturation behavior. Degenerate four-wave mixing results in reduced dimensional systems,[24,25] including an E_{11} study,[8] have reported intensity-dependent dephasing rates, as noted above.

Therefore, we have modeled the observed pump−probe response (Figure 3) by eqs 2 and 3. Aside from the pure dephasing time scale, T_2^*, all of the other material and experimental parameters required for this fitting procedure can be well-estimated or determined; ω (571 nm), ℓ (1 mm), n (1.33), OD (0.15), $|\mu_{22}/e|^2$ (0.9×10^{-14} cm^2), ρ^0 (1.6×10^{14} cm^{-3}), and I^o_{probe}. The overlap of the pump and probe beams for this experimental configuration yields a value of 0.9 for C_θ. The maximum amplitudes of the field envelopes are given for the 1/e field values averaged over the experimental path length (not corrected for attenuation). As indicated above, the observed population decays exhibit multiple time scales over the observed 50 ps interpulse delay range. However, at short times relevant to the description of the coherence relaxation probed by 38 fs pulses, an initial single 315 fs lifetime exponential decay is observed for all fluences, and this is the T_1 value used in this analysis. Lastly, the contribution of inhomogeneous broadening to these FIDs is obtained by modeling the absorption spectrum by a Gaussian distribution of transition frequencies, Δ_{in}. The fitting procedure is constrained such that the convolution of the total dephasing rate, γ_2 and Δ_{in}, results in an absorption bandwidth that matches the observed E_{22} fwhm 94 meV (750 cm^{-1}). Such a description is only approximate because the observed absorption band shapes (E_{11} and E_{22}) are asymmetric. However, the magnitude of this parameter serves to capture the leading t^2 dependence of the FID decay (eq 3). For the subpulse width delay τ = 20 fs data analyzed here, both sequential and interleaving (or coherence coupling) density matrix time histories[13] described above are included in this $\Delta T/T_o$ fitting analysis.

For pump fluences $<\sim 10^{15}$ photons/cm^2, the differential probe transmission of the (6,5) SWNT solution at τ = 20 fs is linearly dependent on the incident pump fluence. Therefore, fitting the $\Delta T/T_o$ expression, modeled as described above in this linear portion of the pump fluence dependence determines a low exciton density, fluence-independent total dephasing time (T_2^o) of 36 fs for the E_{22} transition. This corresponds to a homogeneous width of 36 meV (290 cm^{-1}). For this homogeneous width (dephasing time), Δ_{in}, constrained by the observed 94 meV E_{22} bandwidth (Figure 1), is 68 meV (548 cm^{-1}). Therefore, the inhomogeneous breadth of the E_{22} transition of our SWNT sample solution is nearly twice that of the homogeneous breadth at low pump fluences.

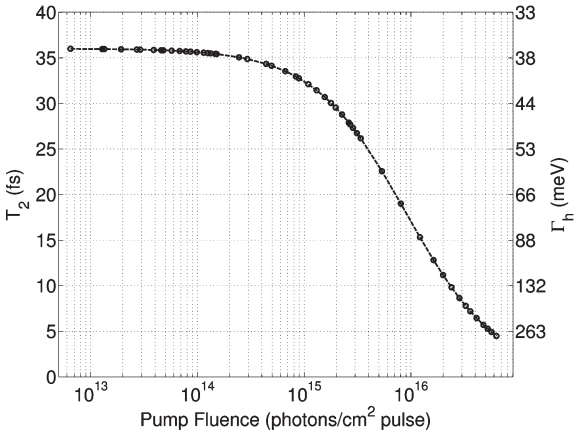

Figure 5. Pump fluence dependence of T_2 determined from the eqs 2 and 5 fit of the $\Delta T/T_o$ data shown in Figure 3.

To fit the observed $\Delta T/T_o$ behavior over the entire pump pulse fluence range, T_2 was given a functional form that depends on the number of excitons created on the nanotube

$$1/T_2(N_x) = 1/T_2^o + \beta_{22}N_x \quad (5)$$

where T_2^o is the fluence-independent, zero exciton total dephasing time (36 fs), and β_{22} represents the linear E_{22} exciton−exciton scattering parameter in this quasi-1D system. N_x is the exciton density per nanotube given by $\sigma_{22}I_{pu}$, where σ_{22} is the E_{22} peak absorption cross-section ($\alpha(cm^{-1})/\rho(SWNT/cm^3)$). This is the form of the dephasing rate used in the previous treatments of the fluence-dependent photon echo decays in other 1D systems.[8−10,24,25] The modeled signal was fit to the data using a least-squares fitting routine, and the resulting best-fit, displayed in Figure 3, is excellent. The observed saturation and decrease in pump−probe intensity with increasing pump fluence are well-captured by this pump-intensity-dependent dephasing model. The best fit β_{22} value is 1.4×10^{-4} μm/fs. A plot of the resulting total dephasing rate as a function of pump fluence for the 38 fs pulses used in this study is given in Figure 5. Because the observed population dynamics (T_1 = 315 fs) is fluence-independent in this early time regime ($\tau \leq$ 300 fs, the quasi-elastic T_2^* component must account for the fluence-dependent dephasing. E_{11} photon echo experiments similarly find a T_2^* pump fluence power dependence.[8−10] The total FID decay has significant contributions from the inhomogeneous (t^2-dependent coherence loss mechanism), as the results above indicate.

Other forms for the fluence dependence of the dephasing rate were used to model the observed $\Delta T/T_o$ signals. For example, we considered just a coherence density dependent form, that is, $1/T_2(N_x) = 1/T_2^o + \eta(N_x)^{1/2}$. However, a dephasing fluence dependence proportional to just E_{pu} ($N_x^{1/2}$) is not sufficient to capture the observed $\Delta T/T_o$ behavior at the largest fluences. The qualitatively similar $\Delta T/T_o$ fluence dependence observed at longer time delays (Figure 4) is attributed to the slow collapse of exciton population to the ground state. For these longer delays (Figure 4), we note that although the E_{22} exciton population has decreased (Figure 2), the majority of excitons have not reached the ground state but remain in the E_{11} manifold.[26]

The β_{22} value (1.4×10^{-4} μm/fs) can be compared with values obtained from photon echo measurements of other

reduced dimensionality (1D) systems, in general, and for the (6,5) E_{11} transition, in particular. As previously pointed out, the β values for the excitons in (6,5) carbon nanotubes are smaller than those found in other systems.[8,24,25] Hence, the effective cross section for exciton−exciton collisions is far smaller for carbon nanotubes than for the analogous quantum wire system. The E_{22} exciton−exciton scattering coefficient β_{22} (room temperature) determined here is about a factor of 6 times smaller than that for the E_{11} transition ($\beta_{11} = 8.1 \times 10^{-4}$ μm/fs) at 130 K[12]. The larger E_{11} exciton−exciton interaction cross-section could be due to a difference in binding energy or exciton size.[27,28]

T_2^o of the E_{11} band is 162 fs, as compared with the E_{22} value of 36 fs determined here. The larger T_2^o and smaller E_{11} effective mass result in a larger exciton diffusion constant. Hence, E_{11} exciton diffusion and Auger annihilation could account for the substantially lower PL saturation fluences reported for (6,5) tubes in solution[18] (10^{14} photons/cm^2), as compared with the E_{22} saturation values reported here and elsewhere.[6] The total dephasing rate at zero exciton density for the E_{22} transition (T_2^o= 36 fs) is, however, notably faster than the dephasing rate found for the E_{11} band (T_2^o = 162 fs).[8] This difference may be due to differences in exciton size, binding energy,[27,28] or exciton−phonon (e−ph) coupling. However, E_{11} and E_{22} exciton binding energies and sizes are not expected to be very different.[27] Studies of the temperature dependence of this low fluence signals can help identify the specific e−ph interactions responsible for this E_{22} dephasing mechanism. Differences in e−ph coupling strengths for the E_{11} and E_{22} transitions have been previously noted.[29]

CONCLUSIONS

The saturation behavior of the differential probe pulse transmission due to the resonant E_{22} exciton transition in an ultrapure room temperature solution of (6,5) carbon nanotubes was obtained and analyzed for pump pulse fluences ranging from 6×10^{12} to 6×10^{16} photons/cm^2. Fits to the third-order polarization treatment described here determine a total dephasing time (T_2^o) of 36 fs in the low fluence regime, corresponding to a homogeneous width of 36 meV (290 cm^{-1}) and a Gaussian-modeled inhomogeneous width of 68 meV (545 cm^{-1}). No change in E_{22} lifetime T_1 is observed for times <300 fs as a function of fluence. Pure dephasing effects dominate T_2 for the E_{22} transition.

Within the framework of this pump−probe description, the extreme $\Delta T/T_o$ saturation and signal quenching effect is attributed to exciton−exciton quasi-elastic scattering ($\beta_{22} = 1.4 \times 10^{-4}$ μm/fs), which results in a fluence-dependent dephasing rate. Only two parameters, T_2^o and β_{22}, are used to fit the observed $\Delta T/T_o$ data over the four orders of magnitude range of the experimental pump fluence. By comparison with the T_2^o for the E_{11} band (162 fs), the low fluence T_2^o (36 fs) for the E_{22} is about a factor of four shorter than that for the E_{11} state, whereas the exciton−exciton scattering parameter, β, is about six times smaller for the E_{22} coherence loss mechanism. Finally, we note that on the basis of the conclusions presented here, the exciton−exciton scattering (β) limits the ability to reach the exciton density required for a Mott transition in these SWNTs by limiting the maximum exciton density that can be reached at these high pump fluences at room temperature.

Future differential transmission studies on this (6,5) system include a more detailed fitting analysis at longer ($\tau > 20$ fs) interpulse delay times and $\Delta T/T$ studies as a function of temperature to verify further this mechanism of signal quenching and identify exciton−phonon contributions to the dephasing of the SWNT transition. More direct studies of the dephasing dynamics may be obtained from two-pulse photon echo measurements using tubes in solutions that offer less scattering,[8] observations made with time-resolved photon echo procedures to help discriminate against scattering background, or both. Photon echo or differential transmission investigations of tubes of other chiralities or other preparations of (6,5) SWNTs would also provide additional tests for the description of coherence dynamics in this high exciton density regime.

APPENDIX

Differential Transmission Signal in Terms of Third-Order Polarization Amplitude. The difference in the energy of a probe beam at a detector after passing through an absorbing sample due to a pump pulse is given in SI units by

$$\Delta I(\tau) = 2n\varepsilon_o c \int_{-\infty}^{\infty} dt\, [|E_{pr}(t) + E_s^{(1)}(t) + E_s^{(3)}(t,\tau)|^2 - |E_{pr}(t) + E_s^{(1)}(t)|^2] \quad \text{(A1)}$$

where $E_s^{(1)}$ and $E_s^{(3)}$ are the linear and nonlinear signal field amplitudes generated by the probe and the pump−probe material responses, respectively, and τ is the time delay between pump and probe pulses. Neglecting any homodyne terms, this change in probe power due to the nonlinear response reduces to

$$\Delta I(\tau) = 4n\varepsilon_o c \mathrm{Re} \int_{-\infty}^{\infty} dt E_{pr}^*(t) E_s^{(3)}(t,\tau) \quad \text{(A2)}$$

The probe pulse energy transmitted through the sample and striking the detector (I_{det}^o) as a result of the linear absorption alone is analogously

$$I_{det}^o = 2n\varepsilon_o c \int_{-\infty}^{\infty} dt\, |E_{pr}(t) + E_s^{(1)}(t)|^2 = 2n\varepsilon_o c \int_{-\infty}^{\infty} dt\, |E_{pr}(t)|^2 + 4n\varepsilon_o c \mathrm{Re} \int_{-\infty}^{\infty} dt\, E_{pr}^*(t) E_s^{(1)}(t) \quad \text{(A3)}$$

The first term above corresponds to the incident probe energy, and the second is the energy absorbed by the sample. Therefore, eq A3 can be rewritten in terms of the incident intensity and the OD

$$I_{det}^o = I_{probe}^o \left(1 - \frac{I_A}{I_{probe}^o}\right) = I_{probe}^o \left(\frac{I_T}{I_{probe}^o}\right) = I_{probe}^o (10^{-\mathrm{OD}}) \quad \text{(A4)}$$

Therefore, in terms of the nonlinear signal field, the differential change in transmitted energy of the probe pulse due to the pump is given by the quotient

$$\frac{\Delta T(\tau)}{T_o} = \frac{\Delta I(\tau)}{I_{det}^o} = \frac{4n\varepsilon_o c \mathrm{Re} \int_{-\infty}^{\infty} dt\, E_{pr}^*(t) E_s^{(3)}(t,\tau)}{I_{probe}^o (10^{-\mathrm{OD}})} \quad \text{(A5)}$$

The signal field can be recast in terms of the corresponding complex third-order polarization amplitude, $E_s^{(3)}(t,\tau) = ((i\omega/n)/(\varepsilon_o c))$-$P^{(3)}(t,\tau)$. (See eq 2.)

■ ACKNOWLEDGMENT

We wish to thank Nick Vamivakas for helpful conversations. We acknowledge support from the National Science Foundation under grants DMR-0706574 (A.G.W. and A.K.S.) and DMR-0520513, EEC-0647560, and DMR-0706067 (A.A.G. and M.C.H.) and CHE-0310497 (L.D.Z.). A.G.W. was supported by a Boston University Photonics Fellowship.

■ REFERENCES

(1) Ostojic, G. N.; Zaric, S.; Kono, J.; Moore, V.; Huage, R. H.; Smalley, R. E. Stability of high density one dimensional excitons in carbon nanotubes under high laser excitation. *Phys. Rev. Lett.* **2005,** *94,* 097401.

(2) Murakami, Y.; Kono, J. Nonlinear photoluminescence excitation spectroscopy of carbon nanotubes: exploring the upper density limit of one-dimensional excitons. *Phys. Rev. Lett.* **2009,** *102,* 037401.

(3) Wang, F.; Dukovic, G.; Brus, L. E.; Heinz, T. F. The optical resonances in carbon nanotubes arise from excitons. *Science* **2005,** *308,* 838.

(4) Maultzsch, J.; Pomraenke, R.; Reich, S.; Chang, E.; Prezzi, D. Exciton binding energies in carbon nanotubes from two-photon photoluminescence. *Phys. Rev. B* **2005,** *72,* 241402(R).

(5) Huang, L.; Krauss, T. D. Quantized bimolecular auger recombination of excitons in single-walled carbon nanotubes. *Phys. Rev. Lett.* **2006,** *96,* 057407.

(6) Luer, L.; Hoseinkhani, S.; Polli, D.; Crochet, J.; Hertel, T.; Lanzani, G. Size and mobility of excitons in (6, 5) carbon nanotubes. *Nat. Phys.* **2009,** *5,* 54.

(7) Ma, Y. Z.; Valkunas, L.; Dexheimer, S. L.; Bachilo, S. M.; Fleming, G. R. Femtosecond spectroscopy of optical excitations in single-walled carbon nanotubes: evidence for exciton-exciton annihilation. *Phys. Rev. Lett.* **2005,** *94,* 157402.

(8) Ma, Y. Z.; Graham, M. W.; Fleming, G. R.; Green, A. A.; Hersam, M. C. Ultrafast exciton dephasing in semiconducting single-walled carbon nanotubes. *Phys. Rev. Lett.* **2008,** *101,* 217402.

(9) Ichida, M.; Kiyohara, Y.; Saito, S.; Miyata, Y.; Kataura, H.; Ando, H. Phase-relaxation processes of excitons in semiconducting single-walled carbon nanotubes. *Phys. Status Solidi* **2008,** *245,* 2712.

(10) Graham, M. W.; Ma, Y.-Z.; Green, A. A.; Hersam, M. C.; Fleming, G. R. Exciton annihilation and dephasing dynamics in semiconducting single-walled carbon nanotubes. *SPIE Proc.* **2010,** *7600,* 76001F-1.

(11) Arnold, M. S.; Green, A. A.; Hulvat, J. F.; Stupp, S. I.; Hersam, M. C. Sorting carbon nanotubes by electronic structure using density differentiation. *Nat. Nanotechnol.* **2006,** *1,* 60.

(12) Ziegler, L. D.; Fan, R.; Desrosiers, A. E.; Scherer, N. F. Femtosecond polarization spectroscopy: a density matrix description. *J. Chem. Phys.* **1994,** *100,* 1823.

(13) Mukamel, S. *Nonlinear Optical Spectroscopy*; Oxford University Press: Oxford, U.K., 1995.

(14) Valkunas, L.; Ma, Y.-Z.; Fleming, G. R. Exciton-exciton annihilation in single-walled carbon nanotubes. *Phys. Rev. B* **2006,** *73,* 115432.

(15) Xiao, Y.-F.; Nhan, T. Q.; Wilson, M. W. B.; Fraser, J. M. Saturation of the photoluminescence at few-exciton levels in a single-walled carbon nanotube under ultrafast excitation. *Phys. Rev. Lett.* **2010,** *104,* 017401.

(16) Green, A. A.; Hersam, M. C. *Mater. Today* **2007,** *10,* 59.

(17) Park, J. Department of Chemistry, Cornell University, Ithaca, NY. Private communication, 2010.

(18) Berciaud, S.; Cognet, L.; Lounis, B. Luminescence decay and the absorption cross section of individual single-walled carbon nanotubes. *Phys. Rev. Lett.* **2008,** *101,* 077402.

(19) Lüer, L.; Gadermaier, C.; Crochet, J.; Hertel, T.; Brida, D.; Lanzani, G. Coherent phonon dynamics in semiconducting carbon nanotubes: a quantitative study of electron-phonon coupling. *Phys. Rev. Lett.* **2009,** *102,* 127401.

(20) Manzoni, C.; Gambetta, A.; Menna, E.; Meneghettti, M.; Lanzani, G.; Cerullo, G. Intersub band exciton relaxation dynamics in single-walled carbon nanotubes. *Phys. Rev. Lett.* **2005,** *94,* 20741.

(21) Loudon, R. *The Quantum Theory of Light*; Oxford University Press: Oxford, U.K., 2000.

(22) Saito, R.; Dresselhaus, G.; Dresselhaus, M. S. *Physical Properties of Carbon Nanotubes*; Imperial College Press: London, 1998.

(23) Tokmakoff, A. Orientational correlation functions and polarization selectivity for nonlinear spectroscopy of isotropic media. I. Third order. *J. Chem. Phys.* **1996,** *105,* 1.

(24) Mayer, E. J.; White, J. O.; Smith, G. O.; Lage, H.; Heitmann, D.; Ploog, K.; Kuhl, J. Femtosecond coherent spectroscopy of etched quantum wires. *Phys. Rev. B* **1994,** *49,* 2993.

(25) Wagner, H. P.; Langbein, W.; Hvam, J. M.; Bacher, G.; Kummell, T.; Forchel, A. Exciton dephasing in ZnSe quantum wires. *Phys. Rev. B* **1998,** *57,* 1797.

(26) Zhu, Z.; Crochet, J.; Arnold, M. S.; Hersam, M. C.; Ulbricht, H.; Resasco, D.; Hertel, T. Pump-probe spectroscopy of exciton dynamics in (6,5) carbon nanotubes. *J. Phys. Chem. C* **2007,** *111,* 3831.

(27) Capaz, R. B.; Spataru, C. D.; Ismail-Beigi, S.; Louie, S. G. Diameter and chirality dependence of exciton properties in carbon nanotubes. *Phys. Rev. B* **2006,** *74,* 121401(R).

(28) Perebeinos, V.; Tersoff, J.; Avouris, P. Scaling of excitons in carbon nanotubes. *Phys. Rev. Lett.* **2004,** *92,* 257402.

(29) Goupalov, S. V.; Satishkumar, B. C.; Doorn, S. K. Excitation and chirality dependence of the exciton-phonon coupling in carbon nanotubes. *Phys. Rev. B* **2006,** *73,* 115401.